ChemPubSoc Europe

DOI: 10.1002/cmdc.201600320

CHEMMEDCHEM Full Papers

BODIPY-Appended 2-(2-Pyridyl)benzimidazole Platinum(II) Catecholates for Mitochondria-Targeted Photocytotoxicity

Koushambi Mitra,[a] Srishti Gautam,[b] Paturu Kondaiah,*[b] and Akhil R. Chakravarty*[a]

Platinum(II) complexes of the type [Pt(L)(cat)] (**1** and **2**), in which H_2cat is catechol and L represents two 2-(2-pyridyl)benzimidazole ligands with 4,4-difluoro-4-bora-3a,4a-diaza-*s*-indacene (BODIPY) pendants, were synthesized to achieve mitochondria-targeted photocytotoxicity. The complexes showed strong absorptions in the range $\lambda = 510–540$ nm. Complex **1** exhibited intense emission at $\lambda = 525$ nm in 1% DMSO/water solution (fluorescence quantum yield of 0.06). Nanosecond transient absorption spectral features indicated an enhanced population of the triplet excited state in di-iodinated complex **2**. The generation of singlet oxygen by complex **2** upon exposure to visible light, as evidenced from experiments with 1,3-diphenylisobenzofuran, is suitable for photodynamic therapy because of the remarkable photosensitizing ability. The complexes resulted in excellent photocytotoxicity in HaCaT cells (half maximal inhibitory concentration $IC_{50} \approx 3$ μM, $\lambda = 400–700$ nm, light dose $= 10$ J cm^{-2}), but they remained non-toxic in the dark ($IC_{50} > 100$ μM). Confocal microscopy images of **1** and Pt estimation from isolated mitochondria showed colocalization of the complexes in the mitochondria. Complex **2** displayed generation of reactive oxygen species induced by visible light, disruption of the mitochondrial membrane potential, and apoptosis.

Introduction

Cisplatin and its analogues are the currently used major chemotherapeutic drugs.[1–3] The mechanism of action of these platinum drugs generally points toward the formation of cross-links with nuclear DNA, which inhibits DNA replication and transcription processes.[4] The present platinum-based drugs suffer from two major disadvantages: a) inherent/acquired drug resistance can occur and b) the drugs cause associated side effects. Thus, for the resurgence of platinum-based anticancer agents to occur, these shortcomings need to be mitigated. Enhanced DNA repair by the nucleotide excision repair (NER) mechanism and increased efflux of the drug are responsible for acquired chemoresistance.[5,6] One possibility for overcoming this drug resistance is to direct the platinum(II) complexes to cellular organelles other than the nucleus. Mitochondria are organelles that regulate metabolic energy, metal homeostasis, apoptotic machinery, and oxidative stress.[7,8] Mitochondria dysfunction is related to cancer progression, so breaking down of the mitochondrial integrity could lead to cellular death. Moreover, mitochondrial DNA (mt-DNA) can serve as a better target for platinum-based drugs because mitochondria lack the NER system and accelerate DNA mutation.[9,10] In fact, cisplatin is also known to deactivate the mitochondrial enzyme thioredoxin reductase and thereby decrease the levels of reduced nicotinamide adenine dinucleotide phosphate (NADPH) and increase cellular reactive oxygen species (ROS) levels.[11]

The side effects also result from uncontrolled hydrolysis of cisplatin en route to the tumor. Various strategies have been adopted to control the pharmacokinetics by altering the ligands and tuning the redox potential of platinum.[1,12,13] It was observed that oxaliplatin and carboplatin reduced the adverse effects and showed improved antiproliferative effects relative to those of cisplatin.[1,2] Thus, replacement of chlorides with bidentate O,O-donor ligands reduced the lability of the metal–donor bonds. Based on these underlying principles, we designed and synthesized platinum(II) complexes that can target mt-DNA in a controlled fashion. We have chosen 4,4-difluoro-4-bora-3a,4a-diaza-*s*-indacene (BODIPY) as the mitochondria-targeting unit because many BODIPY conjugates are well documented to target the mitochondria of cancer cells.[14–16] Moreover, their robust photostability and structural integrity in the tumor microenvironment contributes to their ideal in vitro fluorogenic properties.[15,17] The introduction of heavy atoms like iodine into the BODIPY core results in excellent photosensitizing abilities.[18–20] Thus, iodinated BODIPY dyes have been explored in photodynamic therapy (PDT) for their ability to generate singlet oxygen in the presence of visible light and molecular oxygen.[20,21] The advantage of PDT as compared with other therapies lies in the photosensitized generation of singlet oxygen selectively in the irradiated cancer cells, which reduces any damage to the non-irradiated normal cells.[22–24] Al-

[a] Dr. K. Mitra, Prof. A. R. Chakravarty
Department of Inorganic and Physical Chemistry,
Indian Institute of Science, Bangalore 560012, Karnataka (India)
Fax: (+91) 80-23600683
E-mail: arc@ipc.iisc.ernet.in

[b] S. Gautam, Prof. P. Kondaiah
Department of Molecular Reproduction, Development and Genetics,
Indian Institute of Science, Bangalore 560012, Karnataka (India)
Fax: (+91) 80-23600999
E-mail: paturu@mrdg.iisc.ernet.in

Supporting information for this article can be found under http://dx.doi.org/10.1002/cmdc.201600320.

though the research groups of Burgess, Nagano, and Ziessel synthesized myriads of BODIPY dyes and reported their diverse photophysical properties,[25–30] BODIPY-tethered metal complexes as theranostic agents remain virtually unexplored.[31–34] With an aim to enhance the efficacy of platinum-based drugs, we have designed and synthesized new BODIPY-appended platinum(II) complexes for achieving mitochondria-targeted dual-action DNA crosslinking and PDT effects (Figure 1). The

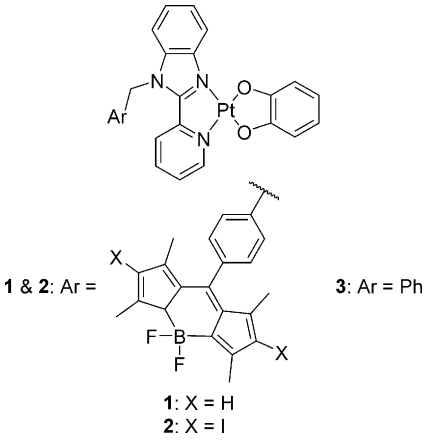

Figure 1. Structures of complexes **1**–**3**.

BODIPY unit linked to 2-(2-pyridyl)benzimidazole binding platinum in a bidentate mode can direct the complexes to the mitochondrial site. After accumulation of the complex, the slow release of the active platinum species inside the cells leads to crosslink formation with the mt-DNA. Based on the previous knowledge, we have chosen catecholate as the O,O-donor ligand to achieve controlled release of the active moieties.

Results and Discussion

Synthesis and general properties

The synthetic versatility of BODIPY was used to design new bidentate ligands and tune their photophysical properties as desired (Scheme S1 in the Supporting Information). A BODIPY precursor (A) containing 2,4-dimethylpyrrole as the core with a chloromethylphenyl substituent at the *meso* position was coupled with the N–H group of 2-(2-pyridyl)benzimidazole to yield ligand L^1 in moderate yield (≈42%). Iodination of L^1 at the alpha position of the BODIPY core with *N*-iodosuccinimide was performed to obtain L^2 (yield ≈54%) as a photosensitizer (PS) for PDT activity. By using these ligands, the dichloro precursor complexes (**1a**–**3a**) of the type $[Pt(L)Cl_2]$ were synthesized from $[Pt(DMSO)_2Cl_2]$. The chlorides were then replaced with catecholate to yield the desired complexes in varying yields (55–88%; Scheme S2 in the Supporting Information). The complexes of formulation [Pt(L)(cat)], in which H_2cat is catechol and L is L^1 in **1** and L^2 in **2**, were characterized and studied for cellular imaging and for their photocytotoxic properties (Figure 1). A non-BODIPY analogue [Pt(L^3)(cat)] (**3**), in which L^3 is 1-benzyl-2-(2-pyridyl)benzimidazole, was prepared and used as a control to study the role of the BODIPY unit in the anticancer activity of **1** and **2**.

The ligands and complexes were characterized by various analytical and spectroscopic methods (Table 1, Figure 2, Figure S1–S16 in the Supporting Information). Mass spectral data indicated the formation of the ligands (Figure S1 and S2 in the Supporting Information). The ^{1}H NMR spectrum of L^1 showed the characteristic peaks of the BODIPY unit at $\delta = 5.8$ ppm for the alpha proton and at $\delta = 2.5$ and 1.2 ppm for the methyl groups (Figure S3a in the Supporting Information). The methylene group proton peaks appeared at $\delta = 6.4$ ppm. The aromatic proton signals appeared in the region $\delta = 7.0$–9.5 ppm. The replacement of the alpha protons by iodine was evident from the absence of the peak at $\delta = 5.8$ ppm in the proton NMR spectrum of L^2 (Figure S4a in the Supporting Information). The ^{13}C NMR spectrum of L^1 showed aromatic carbon atom peaks in the region $\delta = 112$–160 ppm (Figure S3b in the Supporting Information). Signals for the aliphatic carbon atoms of the methylene and methyl groups were observed at $\delta = 49$ and 15 ppm, respectively. Two new peaks at $\delta = 29$ and 87 ppm were observed in the ^{13}C NMR spectrum of L^2 and correspond to the carbon atoms attached to the iodine atoms (Figure S4b in the Supporting Information). The precursor platinum(II) chloro complexes were isolated and characterized by

Table 1. Selected physicochemical data for complexes **1**–**3** and ligands L^1 and L^2.

	1	**2**	**3**	L^1	L^2
λ_{max} [nm] ($\times 10^{-4}\,\varepsilon$ [$M^{-1}\,cm^{-1}$])[a]	510 (1.6), 325 (1.0)	550 (1.37), 525 (1.1), 394 (0.55), 315 (0.93)	530 (0.28), 335 (1.1), 314 (1.2)	505 (2.21), 310 (1.58)	550 (2.16), 388 (0.88), 315 (1.5)
λ_{em} [nm] (Φ_f)[b]	505 (0.06)	–	–	505 (0.12)	–
τ_f [ns][c]	29.6	–	–	27.3	–
τ_T [μs] (Φ_T)[d]	–	2.62 ± 0.01 (0.15)	–	–	3.83 ± 0.06 (0.27)
Λ_M [$S\,m^2\,M^{-1}$][e]	35	32	35	–	–
E_f [V] (ΔE [mV])[f]	1.09, 0.48 (65), −1.13 (190)	1.10, 0.50 (70), −1.3, −0.82	1.03, 0.51 (90), −1.26 (90)	−1.09 (90)	−0.82 (100)

[a] In 10% DMSO/DPBS. [b] In 1% DMSO/DPBS (Fluorescence quantum yield with respect to fluorescein, excitation wavelength = 480 nm). [c] Fluorescence lifetimes measured in 1% DMSO/DPBS (pH 7.2). [d] Triplet-state lifetime obtained from nanosecond time-resolved transient difference absorption spectra in deaerated DMF solutions. [e] Molar conductivity in DMF at $T = 25\,^{\circ}C$. [f] The potentials are versus a saturated calomel electrode (SCE) in DMF/0.1 M TBAP at a scan rate of 100 $mV\,s^{-1}$.

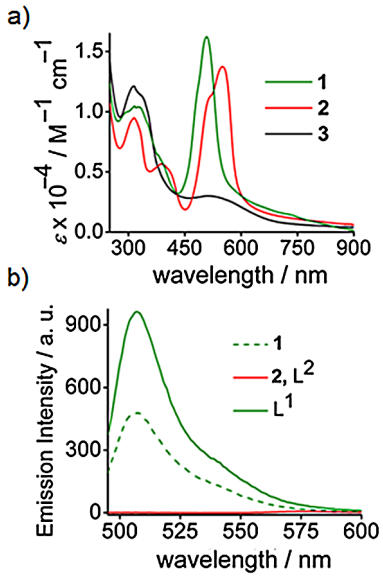

Figure 2. a) Absorption spectra of complexes **1**–**3** (25 μM) and b) emission spectra (λ_{ex} = 480 nm) of complexes **1** and **2** and ligand L^1 in 1% DMSO/DPBS solution (pH 7.2).

both NMR spectroscopy and mass spectral methods (Figure S5–S8 in the Supporting Information). Complexes **1**–**3** displayed additional peaks in the proton NMR spectra at δ = 6.0–6.5 ppm that were assignable to the hydrogen atoms of the catecholate moiety (Figure S9–S11 in the Supporting Information). The peaks in complexes **1** and **2** within the range δ = 6.1–9.2 ppm correspond to the protons of the BODIPY fragment that are not affected by the presence of the metal because they were separated from the platinum coordination sphere by the benzyl spacer moiety. Thus, the BODIPY part was expected to retain its photophysical properties in the complexes. Complex **3** showed peaks only in the aromatic region and for the methylene protons (Figure S11 in the Supporting Information).

The observed peaks in the mass spectra at *m/z* 835.22, 1085.98, and 589.12 for complexes **1**–**3** are in agreement with the calculated *m/z* values for the $[M+H]^+$ species. The isotopic distribution suggested the presence of platinum in the fragments (Figure S12 in the Supporting Information). The purity of the complexes was confirmed from elemental and inductively coupled plasma mass spectrometry (ICP-MS) analytical data. The complexes showed spectral properties similar to those of the ligands (Figure 2a, Figure S13 in the Supporting Information). Complexes **1** and **2** displayed strong absorption bands in 1% DMSO/Dulbecco's phosphate-buffered saline (DPBS; pH 7.2) at λ = 510 ($\varepsilon = 1.61\times10^4\ M^{-1}cm^{-1}$) and 550 nm ($\varepsilon = 1.37\times10^4\ M^{-1}cm^{-1}$), respectively, which were assignable to the electronic transitions involving the BODIPY unit. The control complex **3** showed a relatively weaker and broad absorption band at around λ = 530 nm ($\varepsilon = 0.28\times10^4\ M^{-1}cm^{-1}$). This was a result of charge transfer from the catecholate to the *N*,*N*-bound platinum(II) center. Complex **1** showed a strong emission signal at λ = 505 nm (λ_{exc} = 480 nm) even in 1% DMSO/DPBS medium, which makes it ideal for cellular imaging studies (Figure 2b). Complex **1** with a fluorescence quantum yield (Φ_f) value of 0.06 mimicked the emission properties of the free ligand L^1 (Φ_f = 0.12). There was a loss in emission intensity in **1**, which is possibly a result of partial quenching by platinum(II). The small Stokes shift observed for **1** is characteristic of the fluorescent BODIPY dyes.[15,16] The fluorescence lifetimes of complex **1** and ligand L^1 in 1% DMSO/DPBS solution were found to be 29.6 and 27.3 ns, respectively. In contrast, complex **2** showed no emission band, which suggests that the presence of the heavy atom iodine promotes efficient intersystem crossing that results in complete quenching of the fluorescence intensity (Figure 2b).[20,21]

Redox chemistry and stability

The redox chemistry of the complexes was studied by cyclic voltammetry with complexes and ligands of 1 mM concentration in DMF solutions and by using 0.1 M tetrabutylammonium perchlorate (TBAP) as the supporting electrolyte (Figure 3, Figure S14–S16 in the Supporting Information). The non-BODIPY

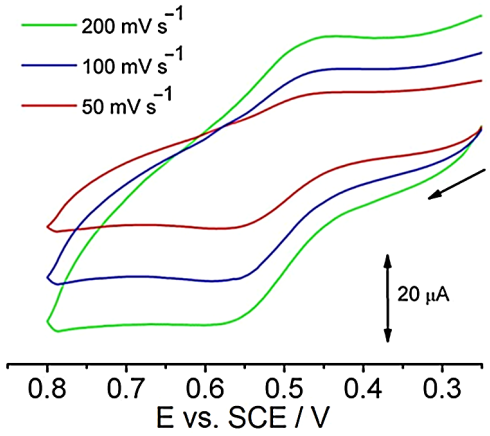

Figure 3. Cyclic voltammograms for complex **2**, showing the anodic response involving the metal-bound catechol moiety, in DMF/0.1 M TBAP at scan rates of 50, 100, and 200 mV s^{-1}.

ligand L^3 was found to be redox inactive within the potential window of the solvent. However, the dichloro precursor platinum(II) complex **3a** displayed a quasireversible cathodic response at a potential of E = −1.15 V and an irreversible anodic peak at E = 1.08 V. These oxidation and reduction processes, therefore, involved the phenyl-substituted 2-(2-pyridyl)benzimidazole ligand coordinated to the platinum(II) center. The cyclic voltammogram of the BODIPY ligand L^1 was dominated by a quasireversible cathodic peak at E = −1.09 V, which is attributed to a reduction involving the BODIPY phenyl-substituted 2-(2-pyridyl)benzimidazole moiety. In the case of the iodinated ligand L^2, the reduction peak was found to be at E = −0.82 V. The observed positive shift of 270 mV is a result of the iodination of the BODIPY core.[35,36] The BODIPY-containing dichloro precursor complexes **1a** and **2a** showed reduction peaks similar to those of free ligands L^1 and L^2. Thus, it was concluded that platinum(II) coordination did not affect the electrogenerat-

ed radical species of the BODIPY core because the introduction of a spacer phenyl ring broke the conjugation. Additional irreversible redox responses were found in **1a** and **2a** at $E = -1.20$ and 1.10 V and were similar to that found in the precursor complex **3a**. The catecholate complexes **1**–**3** exhibited an additional reversible response near $E = 0.5$ V relative to the redox profile of the respective dichloro precursor complexes (Figure 3). Therefore, this couple was assigned to the catecholate and semiquinone radical species; this is a well-known characteristic of the catecholate complexes.[37,38]

The complexes were readily soluble in polar solvents like MeOH, MeCN, DMSO, and DMF. The stability of the complexes was studied (25 μM in 1% DMSO/DPBS, pH 7.2) by monitoring the changes in the absorption spectra with time. It was observed that the complexes were stable in the dark for 48 h. There was no apparent change in their absorption spectra upon photoirradiation for 1 h ($\lambda = 400$–700 nm, light dose = 10 J cm^{-2}), which indicated their photostability (Figure S17 in the Supporting Information).

Transient absorption spectra

We next studied the nanosecond time-resolved transient difference absorption spectra in order to elucidate the dynamics of the triplet excited states of the complexes and ligands (Figure 4, Figure S18 in the Supporting Information). The diiodinated BODIPY complex **2** exhibited a bleaching band at $\lambda = 535$ nm upon nanosecond pulsed laser excitation; this band was a result of depletion of the ground-state population of the BODIPY unit upon excitation. Significant bleaching was also observed for the band at $\lambda = 388$ nm, which was assignable to the BODIPY moiety. A strong transient absorption band at $\lambda = 480$ nm was noted, along with weak absorption bands at $\lambda = 320$ and 340 nm. Broad absorption bands were observed within the range $\lambda = 600$–700 nm. These excited-state spectral features indicate an enhanced triplet-state population, which is localized on the BODIPY part.[39–41] The diiodinated ligand L^2 gave transient absorption profiles similar to those of complex **2**. Under the same experimental conditions, neither complex **1** nor L^1 displayed significant excited-state absorption intensities. The result indicates that iodination of the BODIPY core increased the lifetime of the excited states and, hence, the triplet manifold was easily accessible in the nanosecond timescale. The triplet-state lifetimes obtained from exponential fitting of the decay curves were (2.62 ± 0.01) and (3.83 ± 0.06) μs for complex **2** and ligand L^2, respectively. From the difference absorbance values of the ground state and the excited state, the triplet-state quantum yields were found to be 15 and 27%, respectively, for complex **2** and ligand L^2.

Singlet oxygen generation

ROS generation is an essential feature of PDT agents.[22–24] It is well documented that BODIPY dyes with iodination or bromination at the core can generate singlet oxygen ($^1O_2$) upon light exposure. Thus, trap experiments were performed with the fluorescent dye 1,3-diphenylisobenzofuran (DPBF) to detect any generation of singlet oxygen by the diiodinated analogue, complex **2**.[42] DPBF (50 μM), if treated with complex **2** (5 μM) in an air-saturated DMF medium and exposed to visible light ($\lambda = 400$–700 nm), showed significant attenuation in both emission and absorption intensities, which indicated photoinduced generation of singlet oxygen (Figure 5, Figure S19 in the Supporting Information). The singlet oxygen quantum yield for this complex was 0.23, whereas that for the free ligand L^2 was 0.48. The complex, as expected, failed to generate any singlet

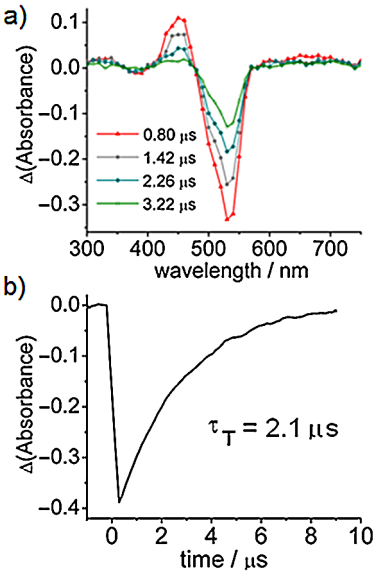

Figure 4. a) Nanosecond time-resolved transient difference absorption spectra and b) first-order exponential decay curve showing the difference in absorbance versus time for complex **2** in aerated DMF with pulsed laser excitation at $\lambda = 532$ nm at room temperature.

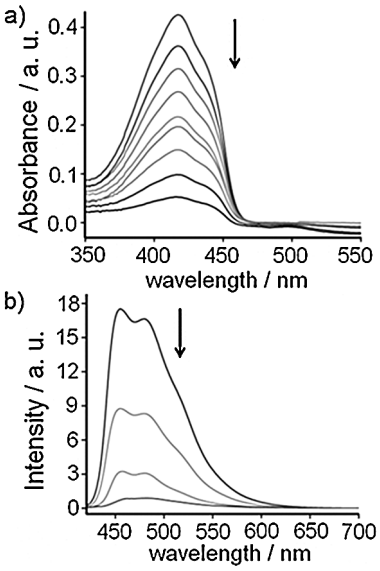

Figure 5. Decrease in a) absorption and b) emission intensity of DPBF (50 μM) in the presence of complex **2** (5 μM) in DMF solution upon photoirradiation ($\lambda = 400$–700 nm). Data recorded at 5 min time intervals of photoexposure.

oxygen species in the absence of light. In contrast, the non-BODIPY analogue complex **3** showed no apparent change in the DPBF intensity under the same photoirradiation conditions (Figure S19 in the Supporting Information).

Theoretical studies

Detailed computational studies were carried out to gain insights into the photophysical properties of the BODIPY complexes **1** and **2** and the non-BODIPY analogue **3**. We employed the B3LYP functional with LanL2DZ as the basis set for all atoms and computation was done with the Gaussian 09 suites.[43–45] The bond lengths and bond angles in the energy-minimized structures were in good agreement with those found in the crystal structures of known platinum catecholates and BODIPY derivatives separately (Table S1 and Figure S20 in the Supporting Information).[46,47] The platinum(II) center adopted a square-planar geometry with Pt–N and Pt–O bond lengths of approximately 2 Å in these complexes. It was observed that the BODIPY core preferred a perpendicular orientation with the phenyl ring at the *meso* position (Figure S20 a,b in the Supporting Information). In such a configuration, the free rotation of the phenyl ring is prohibited because of steric hindrance of the aromatic proton with the adjacent protons of the 1,7-dimethyl groups. This restricts the extended π conjugation and diminishes the probability of non-radiative decay of the excited states of the BODIPY. The calculated HOMO–LUMO energy gaps for complexes **1** and **2** were 1.40 and 1.09 eV, respectively. The decrease in the HOMO–LUMO energy gap in complex **2** is a result of the incorporation of iodine and explains the redshift observed in the absorption spectra of complex **2**. The lower HOMO–LUMO energy difference is in accordance with the varying reduction potentials of the BODIPY-centered reductions in complexes **1** and **2**, as observed in the cyclic voltammetric studies. These energy-minimized structures were further subjected to time-dependent DFT (TDDFT) calculations with the B3LYP/LANL2DZ level of theory to rationalize the nature of the transitions in the visible region and the orbital contributions. Selected singlet transitions and their oscillator strength (*f*) values are tabulated in Table S2 in the Supporting Information. It was deduced that the BODIPY-containing complexes **1** and **2** showed transitions ($f=0.7$) at $\lambda=600$ nm originating from ligand-to-metal charge transfer that involved orbitals localized on the catecholate and platinum(II). A strong transitions with $f=0.34$ was seen at $\lambda=465$ nm, which was assigned to intraligand charge transfer characterized by chief orbital contributions localized on the BODIPY unit (Figure 6, Figure S21 a–c in the Supporting Information). Increased electron densities of the molecular orbitals involved in transitions were found in **2** relative to those in the non-iodinated analogue **1**. The orbitals localized on the iodine atoms, which suggests they have vital roles in the excited-state behavior of the molecules (Figure S21 b,c in the Supporting Information). Interestingly, complex **3**, with no BODIPY pendant, showed very weak transitions in the visible region ($f=0.01$; Figure S21 d in the Supporting Information). The calculated results therefore indicate that the introduction of the BODIPY moiety resulted in strong absorption bands in the visible region of complexes **1** and **2**. The electronic structures of the triplet excited states for complex **2** were obtained by TDDFT studies based on the energy-minimized ground-state geometry. It is clear that the low-lying triplet states are characterized by maximum orbital contributions from the HOMO-8 and LUMO (Figure S22 in the Supporting Information). Electron density analysis of these molecular orbitals concluded that the triplet states are localized on the BODIPY unit, which explains the experimental findings in the nanosecond transient absorption spectral studies.

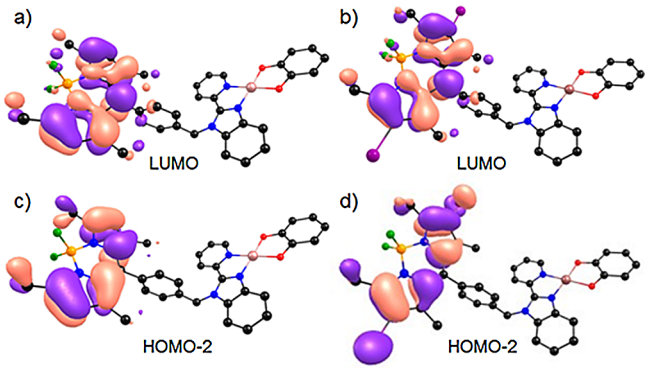

Figure 6. Frontier molecular orbitals involved in the transitions in the visible region for complexes **1** (a and c) and **2** (b and d), as obtained from DFT and TDDFT calculations with the B3LYP/LANL2DZ level of theory. Color codes: Pt: brown; I: pink; F: green; O: red; N: blue; C: black; B: yellow. Hydrogen atoms are omitted for brevity.

MTT assay

The light-induced antiproliferative activities of the complexes were investigated in tumor cell cultures by in vitro experiments. HaCaT human skin keratinocyte cells were chosen for our studies because photoinduced therapies are relevant for easily accessible exposed tissues like skin. The cells were pretreated with the complexes for a short incubation time of 4 h and the cytotoxicities were evaluated in the light and the dark by a 3-(4,5-dimethylthiazol-2-yl)-2,5-diphenyltetrazolium bromide (MTT) assay (Table 2, Figure 7). MTT gets reduced by intercellular oxidoreductase enzymes into insoluble formazan, the level of which directly correlates with the cell viability.[48] Complex **2** showed a prominent dose-dependent loss in the survival rate in HaCaT cells only when illuminated, with a low

Table 2. IC_{50} values in HaCaT cells and mitochondrial Pt uptake of the complexes **1**–**3**.

Complex	IC_{50} [μM][a]		Pt [ng (ng mitochondria)$^{-1}$][c]
	Light[b]	Dark	
1	35.0 ± 5.0	> 100	1.05 ± 0.35
2	2.9 ± 0.3	> 100	1.29 ± 0.21
3	> 100	> 100	–

[a] HaCaT cells treated with complexes for 4 h in the dark. [b] Visible light ($\lambda=400$–700 nm, light dose = 10 J cm^{-2}). [c] HaCaT cells were treated with complexes (100 μM) and the platinum content was determined by ICP-MS methods.

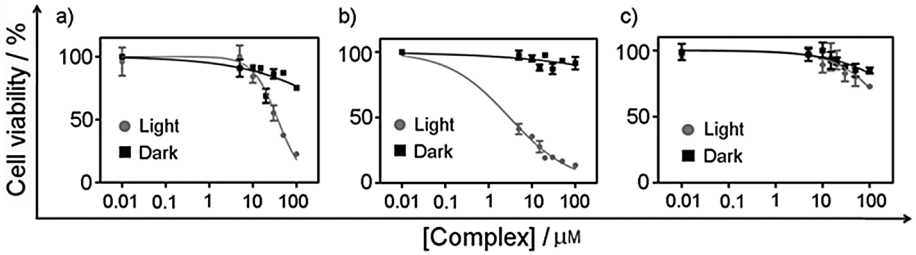

Figure 7. Cell viability plots as obtained from the MTT assay in HaCaT cells treated with complexes **1** (a), **2** (b), and **3** (c) for a 4 h incubation period. Cells were either exposed to light (light gray symbols, $\lambda = 400–700$ nm, light dose = 10 J cm^{-2}) or kept in the dark (black symbols).

half-maximal inhibitory concentration (IC_{50}) value of approximately 3 μM in visible light ($\lambda = 400–700$ nm, light dose = 10 J cm^{-2}) and with no apparent toxicity in the dark ($IC_{50} >$ 100 μM in the dark). Interestingly, the emissive complex **1** gave a high IC_{50} value of approximately 35 μM in visible light under similar treatment conditions. This reflects the crucial role of the iodine on the BODIPY core in augmenting the photosensitizing effect. The low toxicity of **1** in the light and dark made it more suitable for cellular imaging. The non-BODIPY complex **3** showed no cellular toxicity even at a higher concentration of 100 μM, which highlights the essential role of the diiodinated BODIPY unit as a photosensitizer in complex **2**. Complexes **1**–**3** showed substantial toxicity in the dark (IC_{50} values of approximately 20 μM) in HaCaT cells that were preincubated with the complexes for a longer incubation period of 24 h (Figure S23 in the Supporting Information). The cellular toxicity exhibited by the non-BODIPY analogue **3** was found to be similar to that of the Pt–BODIPY conjugates **1** and **2**. This indicated slow dissociation of the Pt–O bonds in the cellular medium, which ultimately led to the formation of lethal Pt–DNA adducts that caused cell death even in the absence of light.[1,2]

Confocal imaging and mitochondrial platinum uptake

The observed PDT effect of **2** made us keen to investigate the mechanism of action. The emissive property of complex **1** in 1% DMSO/DPBS buffer was used to track its key cellular targets. HaCaT cells were treated with **1** (10 μM) and incubated for 4 h in the dark prior to a confocal microscopy study. Propidium iodide (PI) was used as the nuclear staining dye. The cytoplasmic distribution of **1** is clearly illustrated by the merged images in Figure 8a (top row). To further evaluate the exact subcellular colocalization, different cell organelle trackers, namely Mito-Tracker Deep Red (MTR), ER-Tracker Red, and Lyso-Tracker Deep Red, were used. The *Z*-stack confocal image of the complex overlaid with that of the MTR revealed predominant colocalization of complex **1** within the mitochondria (Figure 8a, second row). The presence of complex **1** in the endoplasmic reticulum was indicated by the yellow color of the overlapped images of the complex and ER-Tracker (first row in Figure S24 in the Supporting Information). However, the green emission of **1** showed no overlap with the Lyso-Tracker Deep Red (last row in Figure S24 in the Supporting Information).

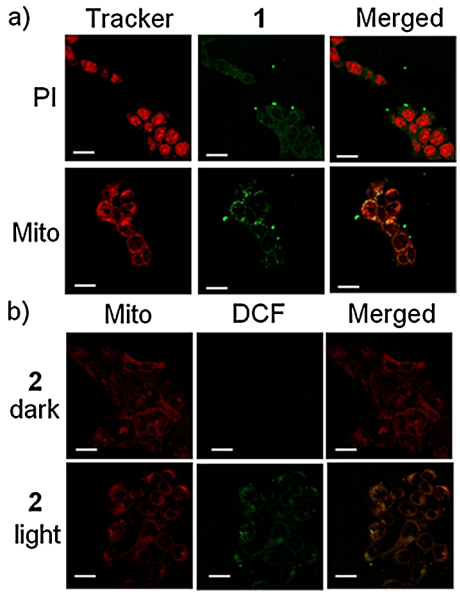

Figure 8. a) Confocal microscopy images of **1** (10 μM) in HaCaT cells after 4 h incubation in the dark. Top row for propidium iodide and second row for Mito-Tracker Deep Red. Merged panels show mitochondrial localization of complex **1**. b) Confocal microscopy images showing generation of ROS at the mitochondrial site by complex **2** upon photoexposure. The formation of DCF is seen from the green intensity in the second column and mitochondrial localization is observed in the merged panels. Scale bar = 25 μm.

The platinum content in isolated mitochondria of HaCaT cells pretreated with the complexes was estimated in order to understand the intercellular fate of the complexes. HaCaT cells were treated with complexes **1**–**3** (100 μM) and incubated for 4 h in the dark. After the treatment, the mitochondria were isolated and the quantity of platinum was estimated by the ICP-MS method. The results are listed in Table 2.[49] It was observed that complexes **1** and **2** both showed substantial platinum content in the mitochondria (1.05 and 1.30 ng of platinum per ng of mitochondria), whereas no platinum was detected for complex **3** in the isolated mitochondria. This indicates the essential role of the BODIPY units for mitochondrial accumulation of the complexes. The combined results from the cellular imaging and platinum estimation studies increased the probability that intact complexes are localizing in the mitochondria.

Dichlorofluorescein diacetate (DCFDA) assay and mitochondrial ROS

The complexes showed light-induced generation of singlet oxygen, as evident from the DPBF studies. Thus, we estimated the cellular ROS amounts in photoexposed HaCaT cells preincubated with the complexes **2** and **3** by a DCFDA assay. The assay is based on the oxidative production of the fluorescent dye dichlorofluorescein (DCF, $\lambda_{em}=525$ nm), the emission intensity of which quantifies the cellular ROS levels.[50] Complex **2** (10 μM) showed significant enhancement in the mean DCF intensity (≈150 a.u.) in light ($\lambda=400$–700 nm, light dose = 10 J cm^{-2}) in the exposed set of cells relative to that of the identical set kept in the dark (Figure S25 in the Supporting Information). However, complex **3** showed similar ROS levels in the dark and light to that in the untreated cells, which confirms its inability to act as a photosensitizer in visible light.

Mitochondria were the key targets of these complexes, so we used confocal imaging to map the subcellular sites of ROS generation. HaCaT cells were treated with complexes **2** and **3** and exposed to light ($\lambda=400$–700 nm, light dose = 10 J cm^{-2}) or kept in the dark. The cells were stained with DCFDA dye (1 μM) for 5 min and images were captured with a Zeiss confocal microscope. Substantial green emission of DCF was observed only in cells treated with complex **2** and subjected to light treatment. Interestingly, the green emission of the produced DCF coincided exactly with the mitochondrial distribution inside the cells (Figure 8b). This showed selective generation of ROS in the mitochondria, which in turn signifies the accumulation of the complexes solely in the mitochondria. The non-BODIPY analogue **3** failed to generate any distinct DCF intensity in both dark and light conditions (Figure S26 in the Supporting Information).

Mitochondrial membrane potential

The mitochondrial ROS formed by complex **2** upon light exposure could lead to alterations in the mitochondrial transmembrane potential ($\Delta\psi_m$).[51,52] The cell-permeant JC-1 dye assembles in mitochondria to form concentration-dependent red-fluorescent J aggregates ($\lambda_{em}=590$ nm). Mitochondrial dysfunction causes a decrease in the $\Delta\psi_m$ value and consequent leakage of JC-1 dye into the cytoplasmic matrix, where it exists as a green-emissive monomer ($\lambda_{em}=530$ nm). This potential-dependent dual emissive property renders JC-1 as a ratiometric probe to monitor any loss of mitochondrial potential.[53] Complex **2** reduced the red-fluorescence intensity with a concomitant increase in the green signal of the JC-1 dye in light-exposed HaCaT cells (Figure S27 in the Supporting Information). Valinomycin (25 μM), which is well documented to depolarize mitochondria, was used as a positive control, with which only the green signal of JC-1 was observed.[54] Complex **3** showed no such changes in cellular images recorded under identical experimental conditions.

Tetramethylrhodamine ethyl ester (TMRE) was employed as a monochromatic probe for measuring the mitochondrial membrane potential with flow cytometry.[55] Membrane-potential-driven accumulation of TMRE in mitochondria results in a strong red fluorescence. Reduction of the emission intensity of TMRE correlates to mitochondrial apoptosis or oxidative-stress-induced depolarization of the mitochondrial membrane. HaCaT cells treated with complex **2** and exposed to light displayed a significant decrease in the TMRE intensity of approximately 350 and 250 a.u., respectively, relative to the treated cells kept in the dark or untreated cells (Figure 9). Valinomycin (25 μM) caused a decrease of 200 a.u. in the TMRE intensity under similar conditions. There was no change in the TMRE intensity in cells treated with complex **3**, which is in agreement with the earlier experimental data.

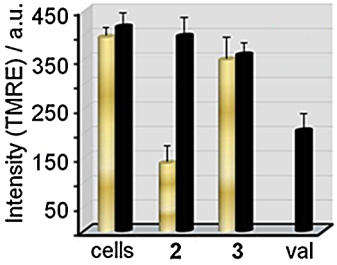

Figure 9. Bar diagram presenting the emission intensity of TMRE in HaCaT cells treated with **2** and **3** for 4 h and then either exposed to light ($\lambda=400$–700 nm; yellow cylinders) or kept in the dark (black cylinders). "Cells" refers to untreated controls and "val" refers valinomycin (25 μM) used as a positive control.

Apoptotic study and cell-cycle assay

It is well established that mitochondrial function governs the intrinsic apoptotic pathway in mammalian cells.[56] The fact that our complexes are perturbing the mitochondrial membrane potential elevates the probability of triggering apoptosis through mitochondrial damage. We examined such a possibility with an annexin-V/fluorescein isothiocyanate (FITC)/propidium iodide (PI) assay with HaCaT cells treated with the complexes under different conditions. The basic principle is selective permeability of the annexin-V/FITC dye toward early apoptotic cells.[57] The percentage population of early apoptotic cells can be inferred from the lower right quadrant of the dot plots in Figure 10a (Figure S28 in the Supporting Information). It was observed that complex **2** showed approximately 50% annexin-V/FITC positive cells only in the presence of light. The complex in the dark resulted in a negligible (≈5%) early apoptotic cell population, which is similar to the result with the untreated controls or cells treated with complex **3** in the dark and light.

The sub-G_1 cell population also relates to the apoptotic population. This cell-cycle phase is characterized by a low DNA content; this DNA can be stained with PI and quantified by a fluorescence-activated cell sort (FACS) analysis.[58] The bar diagram in Figure 10b, obtained from the statistical analysis of the histograms (Figure S29 in the Supporting Information), shows a 59% increase in the sub-G_1 cell population for HaCaT cells treated with complex **2** that were photoirradiated ($\lambda=$ 400–700 nm) relative to the population in those unexposed to

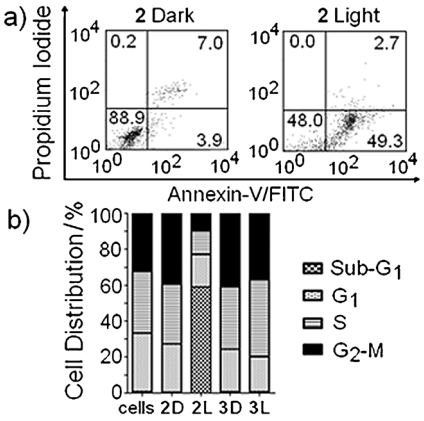

Figure 10. a) Dot plots obtained from the annexin-V/FITC/PI assay with HaCaT cells treated with complex **2** and exposed to light ($\lambda = 400–700$ nm) or kept in the dark. The percentage cell population is given in the respective quadrants: Lower left: live cells; lower right: early apoptotic cells; upper right: late apoptotic/necrotic cells; upper left: dead cells. b) Cell-cycle analysis with propidium iodide staining in HaCaT cells incubated with complexes **2** and **3** for 4 h and exposed to light ($\lambda = 400–700$ nm). The bar diagram represents the percentage cell population in different phases of cell-cycle progression as indicated in the figure. D: dark; L: light ($\lambda = 400–700$ nm). Errors are within $\pm 5\%$.

light. Complex **3**, because of its non-toxic nature, showed a behavior that was similar to that of the untreated controls.

Conclusions

In this work, we have successfully exploited the BODIPY unit to direct bifunctional platinum(II) complexes to target mitochondria. The choice of bidentate catecholate as an O,O-donor ligand ensured slow release of the active platinum(II) species that are capable of forming crosslinks with mt-DNA. The strong emissive properties of complex **1** upon cellular uptake and the high mitochondrial Pt content confirmed accumulation of the complexes in the mitochondria. Incorporation of two iodine atoms in the BODIPY moiety of complex **2** led to an enhanced triplet population in the photoexcited state, which resulted in higher singlet oxygen production in visible light. The photosensitizing ability of complex **2** resulted in a remarkably low IC_{50} value of approximately 3 μM in HaCaT cells in visible light ($\lambda = 400–700$ nm) relative to that with complex **1**. Importantly, these complexes were completely ineffective in the dark and so fulfill the essential criteria for PDT agents. The detailed mechanistic studies in HaCaT cells revealed light-dependent generation of ROS leading to mitochondrial membrane depolarization and the intrinsic apoptotic pathway. This work highlights the tuning of photophysical properties of BODIPY-appended platinum(II) complexes for achieving photoinduced mt-DNA damage. The results are of importance because paradigm shifts from targeting nuclear DNA to mt-DNA and of spatiotemporal control over tumor destruction are necessary to counter drug resistance and minimize the side effects of an anticancer agent.

Experimental Section

Chemicals and experimental methods: Potassium tetrachloroplatinate was purchased from Arora Matthey, India. Mito-Tracker® Deep Red FM, ER-Tracker™ Red, and Lyso-Tracker Deep Red were purchased from Invitrogen (USA). All other chemicals and reagents are obtained from S. D. Fine Chemicals, India, and Sigma–Aldrich, USA. TBAP (0.1 M) was obtained by treating tetrabutylammonium bromide with perchloric acid. [Caution! This reaction must be carried out with proper safety measures.] Solvents were purified in accordance with earlier literature reports.[59] Ligand L^3, precursor compound A, and $Pt(DMSO)_2Cl_2$ were prepared in accordance with earlier reports.[60–62] Platinum(II) catecholates were synthesized by a modified version of a method reported earlier.[63] Elemental analysis was carried out with a Thermo Finnigan Flash EA 1112 CHNS analyzer. NMR spectra were recorded by using a Bruker Avance NMR spectrometer. Mass spectral data were acquired with an Agilent 6538 Ultra High Definition Accurate Mass-Q-TOF (LC-HRMS) instrument. IR, UV/Vis, and emission spectra were recorded with Bruker Alpha and Perkin–Elmer Spectrum 750 spectrophotometers and a HORIBA Jobin Yvon IBH TCSPC fluorimeter (fitted with FluoroHub software analysis). The fluorescence lifetimes were measured with an IBH DataStationHub fluorimeter and fitted by using HORIBA Jobin Yvon decay software. Cyclic voltammetric studies were performed with an EG&G PAR Model 253 VersaStat potentiostat/galvanostat consisting of a three-electrode setup (glassy carbon electrode as the working electrode, a platinum wire as the auxiliary electrode, and a SCE as the reference). Ferrocene was used as a standard. TBAP (0.1 M) was used as a supporting electrolyte. All experiments requiring light exposure were carried out with broad-band white light from a Luzchem Photoreactor (Model LZC-1, Ontario, Canada) fitted with eight fluorescent Sylvania white tubes ($\lambda = 400–700$ nm). Cytotoxic data were obtained with a TECAN microplate reader and fitted by using GraphPad Prism 5 software. Flow cytometric experiments were performed by using a FACS Verse instrument (BD Biosciences) fitted with a MoFLo XDP cell sorter and analyzer with three lasers ($\lambda = 488$, 365, and 640 nm) and ten-color parameters. Confocal microscopy images were acquired by using a Leica microscope (TCS, SP5) with an oil immersion lens with magnification of 63×. Images were processed by using LAS AF Lite software.

Syntheses: The ligands and the complexes were synthesized by using the procedures that are detailed below (Scheme S1 and S2 in the Supporting Information).

Ligand L^1: A mixture of compound A (500 mg, 1.34 mmol), K_2CO_3 (370 mg, 2.68 mmol, 2 equiv), and KI (445 mg, 2.68 mmol, 2 equiv) was placed in aqueous acetonitrile (1:2 v/v, 30 mL) and purged with nitrogen for 15 min. 2-(2-Pyridyl)benzimidazole (209 mg, 1.07 mmol, 0.9 equiv) was added and the solution was heated at reflux at $T = 100\,^{\circ}C$ for 24 h under a nitrogen atmosphere. The solution was then cooled to ambient temperature, diluted with dichloromethane, and washed with water and brine. The organic phase was collected, dried over sodium sulfate, filtered, and evaporated with a rotary evaporator. The crude product thus obtained was purified by silica gel column chromatography by eluting with chloroform/ethyl acetate (9:1 v/v) to yield the desired orange-colored product. Yield = 300 mg (0.56 mmol, 42%); ^1H NMR ($CDCl_3$, 400 MHz): $\delta = 9.19–9.17$ (m, 2H), 8.75–8.69 (m, 1H), 8.33 (t, $J_1 = 4.4$ Hz, $J_2 = 3.6$ Hz, 1H), 8.10 (d, $J = 8$ Hz, 1H), 7.96 (br, 1H), 7.55 (m, 3H), 7.31 (t, $J_1 = 8$ Hz, $J_2 = 2.8$ Hz, 1H), 6.99 (m, 2H), 6.41 (d, $J = 2.4$ Hz, 2H), 5.94 (s, 2H), 2.528 (s, 6H), 1.19 ppm (s, 6H); ^{13}C NMR (100 MHz, $CDCl_3$): $\delta = 156$, 149, 143, 137, 129, 128, 127, 124, 121, 111, 49, 15 ppm; UV/Vis (10% DMSO/DPBS at pH 7.2): λ_{max} (ε) =

505 nm (2.2×10^4 $M^{-1}cm^{-1}$); emission spectrum (10% DMSO/DPBS at pH 7.2): λ_{em} (λ_{ex}, Φ_f) = 505 nm (480 nm, 0.12); elemental analysis: calcd for $C_{32}H_{28}BF_2N_5$: C 72.33, H 5.31, N 13.18; found: C 72.10, H 5.07, N 13.06; molecular weight = 531.41 g mol^{-1}; MS (MeOH): *m/z* 532.24 $[M+H]^+$.

Ligand L^2: Ligand L^1 (0.70 gm, 1.31 mmol) was placed in dry dichloromethane (50 mL) and degassed with bubbling nitrogen. An excess of *N*-iodosuccinimide (1.80 gm, 8 mmol, 6 equiv) was added and the mixture was stirred for 12 h under a nitrogen atmosphere. The red solution was diluted with dichloromethane and washed with water. The organic phase was dried over sodium sulfate, filtered, and evaporated with a rotary evaporator. The crude product was subjected to silica gel column chromatography by using chloroform/ethyl acetate (9:1 v/v) to afford a pink-red solid. Yield = 550 mg (0.7 mmol, 54%); ^{1}H NMR ($CDCl_3$, 400 MHz): δ = 9.19 (m, 2H), 8.74 (m, 1H), 8.34 (d, J = 8.0 Hz, 1H), 8.14 (t, J_1 = 8.0 Hz, J_2 = 8 Hz, 2H), 7.65–7.59 (br, 3H), 7.57 (d, J = 4.0 Hz, 1H), 7.25 (m, 2H), 6.42 (s, 2H), 2.63 (d, J = 4 Hz, 6H), 1.22 ppm (s, 6H); ^{13}C NMR (100 MHz, [D$_6$]DMSO/$CDCl_3$ (1:1)): δ = 156, 149, 145, 141, 139, 138, 133, 131, 128, 125, 124, 119, 112, 87, 49, 29, 16 ppm; UV/Vis (10% DMSO/DPBS at pH 7.2): λ_{max} (ε) = 550 (2.17×10^4), 515 (1.75×10^4), 388 nm (0.9×10^4 $M^{-1}cm^{-1}$); elemental analysis: calcd for $C_{32}H_{26}BF_2I_2N_5$: C 49.07, H 3.35, N 8.94; found: C 48.90, H 3.56, N 8.90; molecular weight = 783.21 g mol^{-1}; MS (MeOH): *m/z* 784.04 $[M+H]^+$.

Preparation of [Pt(L)Cl$_2$] (1a–3a): The precursor complex [Pt(DMSO)$_2$Cl$_2$] was mixed with the appropriate ligand (1 equiv) in degassed acetonitrile (30 mL) and the reaction was heated at reflux for 24 h under a nitrogen atmosphere. Upon cooling of the reaction mixture to 0 °C, a precipitate was obtained, which was filtered and washed thoroughly with hexane and diethyl ether.

Complex [Pt(L^1)Cl$_2$] (1a): [Pt(DMSO)$_2$Cl$_2$] (78 mg, 0.188 mmol), L^1 (100 mg, 0.188 mmol); yield = 132 mg (0.16 mmol, 88%); ^{1}H NMR ([D$_6$]DMSO, 400 MHz): δ = 9.63 (d, J = 6 Hz, 2H), 9.08 (d, J = 8.4 Hz, 1H), 8.24 (t, J_1 = 8.8 Hz, J_2 = 7.6 Hz, 1H), 8.11–8.04 (dd, J_1 = 8.4 Hz, J_2 = 8.8 Hz, J_3 = 8.0 Hz, 1H), 7.77 (t, J_1 = 6.4 Hz, J_2 = 7.2 Hz, 2H), 7.64–7.49 (m, 2H), 7.36–7.29 (m, 3H), 6.32 (s, 2H), 6.17 (d, J = 16.4 Hz, 2H), 1.35 (s, 6H), 1.18 ppm (s, 6H); elemental analysis: calcd for $C_{32}H_{28}BCl_2F_2N_5Pt$: C 48.20, H 3.54, N 8.78; found: C 48.06, H 3.72, N 8.52; molecular weight = 797.40 g mol^{-1}; MS (MeOH): *m/z* 819.12 $[M+Na]^+$, 761.17 $[M-Cl]^+$.

Complex [Pt(L^2)Cl$_2$] (2a): [Pt(DMSO)$_2$Cl$_2$] (132 mg, 0.32 mmol), L^2 (250 mg, 0.32 mmol); yield = 130 mg (0.12 mmol, 50%); ^{1}H NMR ([D$_6$]DMSO, 400 MHz): δ = 9.65 (d, J = 5.6 Hz, 1H), 9.08 (d, J = 8.4 Hz, 1H), 8.27 (t, J_1 = J_2 = 8.0 Hz, 1H), 8.07 (t, J_1 = 8.4 Hz, J_2 = 5.2 Hz, 1H), 7.81 (t, J_1 = 8.4 Hz, J_2 = 6.8 Hz, 1H), 7.56 (t, J_1 = 8 Hz, J_2 = 7.6 Hz, 1H), 7.41–7.34 (m, 6H), 6.33 (s, 2H), 1.19 ppm (m, 12H); elemental analysis: calcd for $C_{32}H_{26}BCl_2F_2I_2N_5Pt$: C 36.63, H 2.50, N 6.68; found: C, 36.40, H 2.63, N 6.32; molecular weight = 1049.19 g mol^{-1}; MS (MeOH): *m/z* 1071.93 $[M+Na]^+$, 1012.96 $[M-Cl]^+$.

Complex [Pt(L^3)Cl$_2$] (3a): [Pt(DMSO)$_2$Cl$_2$] (333 mg, 0.792 mmol), L^3 (225 mg, 0.792 mmol); yield = 365 mg (0.66 mmol, 83%); ^{1}H NMR ([D$_6$]DMSO, 400 MHz): δ = 9.63 (d, J = 6.0 Hz, 1H), 9.04 (d, J = 8.4 Hz, 1H), 8.30 (t, J_1 = J_2 = 8.0 Hz, 1H), 8.15 (d, J = 7.6 Hz, 1H), 7.94 (d, J = 8.4 Hz, 1H), 7.77 (t, J_1 = 6.4 Hz, J_2 = 6.8 Hz, 1H), 7.59–7.50 (m, 2H), 7.37–7.28 (m, 3H), 7.19 (d, J = 7.2 Hz, 2H), 6.18 ppm (s, 2H); elemental analysis: calcd for $C_{19}H_{15}Cl_2N_3Pt$: C 41.39, H 2.74, N 7.62; found: C 41.19, H 2.86, N 7.51; molecular weight = 551.33 g mol^{-1}; MS (MeOH): *m/z* 573.01 $[M+Na]^+$, 515.06 $[M-Cl]^+$.

Preparation of [Pt(L)(cat)] (1–3): The appropriate dichloroplatinum complex [Pt(L)Cl$_2$] was mixed with catechol (1 equiv) and cesium carbonate (2 equiv) in methanol (20 mL) and heated at reflux for 6 h in the dark under a nitrogen atmosphere. The solvent was then evaporated to dryness and the residue was dissolved in DMF (2 mL). The desired complex was precipitated by adding excess diethyl ether and was repeatedly washed with water and diethyl ether to remove any unreacted starting materials.

Complex [Pt(L^1)(cat)] (1): [Pt(L^1)Cl$_2$] (100 mg, 0.12 mmol), catechol (17 mg, 0.15 mmol), Cs_2CO_3 (90 mg, 0.25 mmol); yield = 50% (brown solid, 50 mg, 0.06 mmol); ^{1}H NMR ([D$_6$]DMSO, 400 MHz): δ = 9.62 (d, J = 7.4 Hz, 2H), 9.08 (d, J = 8 Hz, 1H), 8.23 (d, J = 7.6 Hz, 1H), 8.11–8.04 (m, 2H), 7.77 (t, J_1 = 7.2 Hz, J_2 = 6.8 Hz, 3H), 7.64–7.32 (m, 1H), 7.33 (d, J = 5.6 Hz, 1H), 6.51 (d, J = 3.2 Hz, 2H), 6.32–6.29 (m, 4H), 6.13 (s, 2H), 2.48 (s, 6H), 1.18 ppm (s, 6H); UV/Vis (10% DMSO/DPBS at pH 7.2): λ_{max} (ε) = 510 (1.6×10^4), 325 nm (1.1×10^4 $M^{-1}cm^{-1}$); emission spectrum (1% DMSO/DPBS at pH 7.2): λ_{em} (λ_{ex}, Φ_f) = 505 nm (480 nm, 0.06); elemental analysis: calcd for $C_{38}H_{32}BF_2N_5O_2Pt$: C 54.69, H 3.68, N 8.39; found: C 54.22, H 3.82, N 8.25; molecular weight = 834.59 g mol^{-1}; MS (MeOH): *m/z* 835.59 $[M+H]^+$.

Complex [Pt(L^2)(cat)] (2): [Pt(L^2)Cl$_2$] (125.9 mg, 0.12 mmol), catechol (17 mg, 0.15 mmol), Cs_2CO_3 (90 mg, 0.25 mmol); yield = 44% (violet solid, 55 mg, 0.05 mmol); ^{1}H NMR ([D$_6$]DMSO, 400 MHz): δ = 9.65 (d, J = 4.9 Hz, 1H), 9.30 (d, J = 5.1 Hz, 1H), 9.07 (d, J = 8.2 Hz, 1H), 8.46–8.44 (m, 1H), 8.31–8.22 (m, 1H), 8.14–8.06 (m, 1H), 7.97 (d, J = 8.8 Hz, 1H), 7.69–7.53 (m, 2H), 7.37–7.34 (m, 1H), 7.21–7.20 (d, J = 7.2 Hz, 2H), 6.61–6.55 (m, 2H), 6.33 (s, 2H), 6.16 (2H, s) 2.54 (s, 6H), 1.18 ppm (s, 6H); UV/Vis (10% DMSO/DPBS at pH 7.2): λ_{max} (ε) = 550 (1.37×10^4), 525 nm (1.10×10^4 $M^{-1}cm^{-1}$); elemental analysis: calcd for $C_{38}H_{30}BF_2I_2N_5O_2Pt$: C 42.01, H 2.78, N 6.45; found: C 41.89, H 2.62, N 6.33; molecular weight = 1049.19 g mol^{-1}; MS (MeOH): *m/z* 1048.94 $[M+H]^+$.

Complex [Pt(L^3)(cat)] (3): [Pt(L^3)Cl$_2$] (275 mg, 0.5 mmol), catechol (65 mg, 0.5 mmol), Cs_2CO_3 (358 mg, 1.1 mmol); yield = 60% (violet solid, 175 mg, 0.3 mmol); ^{1}H NMR ([D$_6$]DMSO, 400 MHz): δ = 9.29 (d, J = 5.6 Hz, 2H), 8.45 (t, J_1 = 2.4 Hz, J_2 = 6.8 Hz, 1H), 8.22 (d, J = 7.6 Hz, 1H), 8.12 (d, J = 8 Hz, 1H), 7.97–7.95 (m, 4H), 7.68–7.19 (m, 2H), 7.61–7.55 (m, 2H), 6.25–6.22 (m, 2H), 6.15 (s, 2H), 5.94 ppm (s, 2H); UV/Vis (10% DMSO/DPBS at pH 7.2): λ_{max} (ε) = 530 (0.3×10^4), 335 nm (1.1×10^4 $M^{-1}cm^{-1}$); elemental analysis: calcd for $C_{25}H_{19}N_3O_2Pt$: C 51.02, H 3.25, N 7.14; found: C 50.84, H 3.36, N 7.10; molecular weight = 588.53 g mol^{-1}; MS (MeOH): *m/z* 589.12 $[M+H]^+$.

Nanosecond time-resolved transient absorption spectroscopy: The difference absorption spectra were recorded by using a laser flash photolysis spectrometer (LKS.60 Applied Photophysics). DMF solutions of the complexes and ligands (20 μM) were purged with argon for 15–30 min prior to the measurements. The solutions were excited with a nanosecond-pulsed laser (532 nm, pulse width of 5–8 ns) and the transient signals were acquired and digitalized with an oscilloscope (54520 A, Hewlett–Packard). The quantum yield was calculated with zinc(II) phthalocyanine (ZnPc) as the reference compound (Φ_T = 0.65).

Detection and quantum yield for singlet oxygen: DPBF showed poor sensitivity for $^1O_2$ in aqueous solutions. It was also prone to photobleaching in halogenated solvents. However, it was photostable in DMF. Therefore, the singlet oxygen quenching experiments were carried out with DMF solutions. The non-emissive complexes **2** and **3** (5 μM) were treated with DPBF (50 μM) in DMF and the emission spectra were recorded at an excitation wave-

length of 405 nm. Either irradiation was performed with 400–700 nm visible light for different time intervals or the samples were kept in the dark. The time-dependent absorption spectral experiments with DPBF and complexes **2** and **3** in DMF were performed in a similar fashion. The quantum yield of singlet oxygen generation (Φ_Δ) was calculated by using the equation: $\Phi_\Delta = \Phi_\Delta^{ref}$ (k/k^{ref})(I_a^{ref}/I_a), in which Φ_Δ^{ref} is the singlet oxygen quantum yield for the reference (Rose Bengal was used as the standard, $\Phi_\Delta = 0.76$), k and k^{ref} are the photobleaching rate constants in the presence of the respective samples and the standard, and I_a and I_a^{ref} are the absorption intensities at the irradiation wavelength (510 nm) of the samples and reference, respectively.[64]

Theoretical calculations: The energy-minimized geometries of complexes **1**–**3** were obtained by the DFT method by employing the B3LYP functional (LANL2DZ basis sets for all atoms) as implemented in the Gaussian 09 program.[43–45] Linear-response TDDFT performed on the optimized structures revealed the energy of transitions along with the oscillator strengths and orbital contributions.

MTT assay: Cytotoxicity studies were done with complexes **1**–**3** in HaCaT (human keratinocyte) cells. Cells were incubated with various concentrations of **1**–**3** (5, 10, 15, 20, 30, 50, and 100 μM in 1% DMSO/Dulbecco's modified Eagle's medium (DMEM)) for 4 h in complete darkness. One set of cells was exposed to visible light ($\lambda = 400$–700 nm, light dose $= 10\ J\,cm^{-2}$), whereas the other was kept in the dark for 1 h. Data were obtained by using three independent sets of experiments done in triplicate for each concentration. Ligands and precursor dichloroplatinum(II) complexes were not studied because they were insoluble in 1% DMSO/DPBS medium (see the Supporting Information for details).

Confocal microscopy and mitochondrial Pt estimation: The intracellular localization of complex **1** was investigated by using a Leica microscope (TCS, SP5) with an oil immersion lens with a magnification of 63×. HaCaT cells were incubated with the complex (10 μM in 1% DMSO/DMEM) in the dark for 4 h. Cells were stained with PI (1 $mg\,mL^{-1}$) for 5 min. Further information on the subcellular localization was obtained by using similar treatment procedures but without any prior fixation of cells by using methanol. Live cells were stained with Mito-tracker® Deep Red (50 nM), ER-Tracker™ Red (50 nM), or Lyso-Tracker Deep Red (50 nM), incubated for 20 min at room temperature, and subsequently visualized under the microscope. Multiple images were recorded and experiments were done in duplicate to confirm the results (see the Supporting Information for details). Approximately 10^6 HaCaT cells were incubated with complexes **1**–**3** (100 μM) for 4 h in the dark. After treatment, the cells were collected and resuspended in mitochondrial isolation buffer (10 mL of 0.1 M tris(hydroxymethyl)aminomethane (Tris)/3-(*N*-morpholine)propanesulfonic acid and 1 mL of ethylene glycol-bis(β-aminoethyl ether)-*N*,*N*,*N*′,*N*′-tetraacetic acid/Tris to 20 mL of 1 M sucrose and volume made up to 100 mL (pH 7.4)). Cells were then homogenized at $T = 4\,^\circ C$ by using a Teflon pestle (1600 rpm) and the cell suspensions were stroked gently in a glass potter (initially cooled in an ice bath to maintain the mitochondrial integrity). The homogenate was centrifuged again at 7000 g at 4 °C for 10 min and the pellet containing the mitochondria was collected. One such set was used for measuring the concentration by Biuret methods and for examining the separation of mitochondria by gel electrophoresis. Another identical set was used for Pt estimation by ICP-MS after dilution in 2% HNO_3/DPBS solutions (see the Supporting Information for details).

DCFDA assay: The photoinduced generation of ROS by complexes **2** and **3** (in 1% DMSO/DMEM) in HaCaT was quantified by using the DCFDA assay. Cells were incubated with the complexes **2** (5 μM) and **3** (20 μM) for 4 h in complete darkness. One of the plates was irradiated ($\lambda = 400$–700 nm, light dose $= 10\ J\,cm^{-2}$) for 1 h in phenol red free medium, whereas the other was kept in the dark. Cells were then washed with DPBS, treated with trypsin (1×), and collected by centrifugation. Cells were resuspended in DPBS, treated with DCFDA (1 μM), and incubated for 15 min at $T = 0\,^\circ C$. Samples were then taken for reading with a FACS Verse machine (BD Biosciences). Untreated controls were kept as references and experiments were done in duplicate. The DCFDA assay was performed by using confocal microscopy for complexes **2** and **3** (in 1% DMSO/DPBS) in HaCaT cells. To visualize the subcellular site of ROS production, Mitotracker® Deep Red (MTR, 50 nM) and DCFDA (1 μM) were used. Cells were plated in 12-well tissue culture plates on cover slips in the usual way for microscopic experiments. Cells were then incubated in the dark for 4 h with complexes **2** (5 μM) and **3** (20 μM). Cells were either photoexposed ($\lambda = 400$–700 nm, $t = 30$ min in phenol red free media) or kept in the dark. The cells were stained with MTR and DCFDA for 20 min at room temperature. The cover slips were mounted and tethered to slides. Images were captured by using a Leica microscope (TCS, SP5) with an oil immersion lens with a magnification of 63×. Multiple images were recorded and experiments were done in duplicate to confirm the results.

Mitochondrial membrane potential JC-1 assay: The dual emissive nature of the JC-1 dye, the differential intensities of which depend on the mitochondrial membrane potential, was employed to further confirm the mitochondrial membrane depolarization. Complexes **2** (5 μM) and **3** (20 μM) in 1% DMSO/DMEM were added to HaCaT cells and incubated for 4 h in the dark. The cells were exposed to light ($\lambda = 400$–700 nm, $t = 1$ h) or kept in the dark in phenol red free media. The confocal images were captured in both red and green channels by using a Leica microscope. Untreated cells served as negative controls, whereas cells treated with valinomycin (25 μM, $t = 1$ h) served as a positive control for the experiments (see the Supporting Information for details).

Mitochondrial membrane potential TMRE assay: To assess the mitochondrial dysfunction, TMRE, a fluorescent dye ($\lambda_{em} = 690$ nm) that exhibits a mitochondrial membrane potential dependent accumulation in mitochondria, was used. HaCaT cells were incubated with complexes **2** (5 μM) and **3** (20 μM) in 1% DMSO/DMEM for 4 h. Cells were either kept in the dark or irradiated with visible light for 1 h in phenol red free medium. Untreated cells and cells treated with valinomycin (25 μM, $t = 1$ h), which is known to depolarize mitochondria, were kept as controls. The FACS analysis of these samples gave a quantitative measure of TMRE intensity (see the Supporting Information for details).

Annexin-V/FITC/PI assay: The early apoptotic cell population was determined for complexes **2** (5 μM) and **3** (20 μM) in 1% DMSO/DMEM. Approximately 3×10^5 HaCaT cells were seeded in six-well plates and cultured for 24 h. The cells were incubated with **2** and **3** for 4 h in the dark and then exposed to light ($\lambda = 400$–700 nm, light dose $= 10\ J\,cm^{-2}$) in phenol red free media or kept in complete darkness. Cells were then kept for another 14 h in DMEM/10% fetal bovine serum (FBS) medium in the dark, after which the medium was discarded and the cells were trypsinized and resuspended in binding buffer (300 μL, 1×). Annexin-V/FITC (0.5 μL) and PI (1 μL) were added to the cell suspensions and incubated for 5 min. Readings were taken with the FACS instrument. Gating of cell population was performed based on the untreated controls.

Experiments were performed in duplicate and data were represented as dot plots.

Cell-cycle analysis: The influence of complexes **2** and **3** on cell-cycle progress was analyzed by this assay. Approximately 1.0×10^6 HaCaT cells were cultured in six-well tissue culture plates in DMEM/10% FBS for 24 h. Then, 1% DMSO/DMEM solutions of complexes **2** (5 μM) and **3** (20 μM) were added to the cells and incubated for 4 h in dark. One of the complex-treated plates was subjected to irradiation in phenol red free media ($\lambda = 400$–700 nm, light dose = 10 J cm^{-2}), whereas the identical other set was kept in the dark. After the irradiation, post-incubation was done for 24 h in the dark. Cells were then processed and analyzed with a FACS Verse machine (BD Biosciences) at the FL2 channel ($\lambda = 595$ nm) and the populations of cells in different phases of the cell cycle were obtained from histograms generated by the Cell Quest Pro software (BD Biosciences). Experiments were performed in duplicate, along with untreated controls.

Acknowledgements

The authors thank the Department of Science and Technology (DST), Government of India, for financial support (grant numbers SR/S5/MBD-02/2007 and EMR/2015/000742). The authors also thank the Alexander von Humboldt (AvH) Foundation, Germany, for an electrochemical system. A.R.C. thanks the DST for a J. C. Bose Fellowship. P.K.'s research group is funded by DBT-IISc grants. K.M. is a recipient of a BMS fellowship. We thank Urvashi and Deepika for FACS data, Saima and Santosh for confocal microscopy images, and Sudeeksh for help in the transient absorption studies. We thank Dr. R. Chakrabarti from CEaS, IISc, for the ICP-MS data.

Keywords: antitumor agents · bioinorganic chemistry · BODIPY · platinum · singlet oxygen

[1] T. C. Johnstone, G. Y. Park, S. J. Lippard, *Anticancer Res.* **2014**, *34*, 471–476.
[2] Q.-Q. Deng, X.-E. Huang, L.-H. Ye, Y.-Y. Lu, Y. Liang, J. Xiang, *Asian Pac. J. Cancer Prev.* **2013**, *14*, 413–417.
[3] World Health Organization, "WHO Model List of Essential Medicines", **2013**.
[4] D. Gibson, *Dalton Trans.* **2009**, 10681–10689.
[5] Ž. D. Bugarčić, J. Bogojeski, B. Petrović, S. Hochreutherb, R. Eldik, *Dalton Trans.* **2012**, *41*, 12329–12345.
[6] A. V. Klein, T. W. Hambley, *Chem. Rev.* **2009**, *109*, 4911–4920.
[7] C. Wang, R. Youle, *Nature* **2016**, *530*, 288–289.
[8] C. Wang, R. J. Youle, *Annu. Rev. Genet.* **2009**, *43*, 95–118.
[9] A. Chatterjee, E. Mambo, D. Sidransky, *Oncogene* **2006**, *25*, 4663–4674.
[10] M.-C. Frantz, P. Wipf, *Environ. Mol. Mutagen.* **2010**, *51*, 462–475.
[11] I. Romero-Canelón, P. J. Sadler, *Inorg. Chem.* **2013**, *52*, 12276–12291.
[12] T. C. Johnstone, K. Suntharalingam, S. J. Lippard, *Chem. Rev.* **2016**, *116*, 3436–3486.
[13] X. Wang, X. Wang, Z. Guo, *Acc. Chem. Res.* **2015**, *48*, 2622–2631.
[14] a) J. Zhao, K. Xu, W. Yang, Z. Wang, F. Zhong, *Chem. Soc. Rev.* **2015**, *44*, 8904–8939; b) T. Kowada, H. Maeda, K. Kikuchi, *Chem. Soc. Rev.* **2015**, *44*, 4953–4972.
[15] a) J. Zhao, W. Wu, J. Sun, S. Guo, *Chem. Soc. Rev.* **2013**, *42*, 5323–5351; b) P. Kos, H. Plenio, *Chem. Eur. J.* **2015**, *21*, 1088–1095.
[16] a) B. C. Wilson, M. Olivo, G. Singh, *Photochem. Photobiol.* **1997**, *65*, 166–176; b) R. Bonnett, *Chemical Aspects of Photodynamic Therapy*, Gordon & Breach, London, **2000**.
[17] N. Boens, V. Leen, W. Dehaen, *Chem. Soc. Rev.* **2012**, *41*, 1130–1172.
[18] A. Kamkaew, S. H. Lim, H. B. Lee, L. V. Kiew, L. Y. Chung, K. Burgess, *Chem. Soc. Rev.* **2013**, *42*, 77–88.
[19] S. Kolemen, M. Işik, G. M. Kim, D. Kim, H. Geng, M. Buyuktemiz, T. Karatas, X.-F. Zhang, Y. Dede, J. Yoon, E. U. Akkaya, *Angew. Chem. Int. Ed.* **2015**, *54*, 5340–5344; *Angew. Chem.* **2015**, *127*, 5430–5434.
[20] a) A. Bhattacharyya, A. Dixit, K. Mitra, S. Banerjee, A. A. Karande, A. R. Chakravarty, *MedChemComm* **2015**, *6*, 846–851; b) S. G. Awuah, Y. You, *RSC Adv.* **2012**, *2*, 11169–11183.
[21] a) S. Guo, L. Ma, J. Zhao, B. Küçüköz, A. Karatay, M. Hayvali, H. G. Yaglioglu, A. Elmali, *Chem. Sci.* **2014**, *5*, 489–500; b) I. S. Turan, D. Yildiz, A. Turksoy, G. Gunaydin, E. U. Akkaya, *Angew. Chem. Int. Ed.* **2016**, *55*, 2875–2878; *Angew. Chem.* **2016**, *128*, 2925–2928.
[22] W. A. Velema, W. Szymanski, B. L. Feringa, *J. Am. Chem. Soc.* **2014**, *136*, 2178–2191.
[23] D. E. Dolmans, D. Fukumara, R. K. Jain, *Nat. Rev. Cancer* **2003**, *3*, 380–387.
[24] M. Ethirajan, Y. Chen, P. Joshi, R. K. Pandey, *Chem. Soc. Rev.* **2011**, *40*, 340–362.
[25] a) A. Kamkaew, K. Burgess, *J. Med. Chem.* **2013**, *56*, 7608–7614; b) A. Kamkaew, K. Burgess, *Chem. Commun.* **2015**, *51*, 10664–10667.
[26] a) L. Wu, K. Burgess, *Chem. Commun.* **2008**, 4933–4935; b) A. Kamkaew, S. Thavornpradit, T. Puangsamlee, D. Xin, N. Wanichacheva, K. Burgess, *Org. Biomol. Chem.* **2015**, *13*, 8271–8276.
[27] a) T. Yogo, Y. Urano, Y. Ishitsuka, F. Maniwa, T. Nagano, *J. Am. Chem. Soc.* **2005**, *127*, 12162–12163; b) T. Komatsu, D. Oushiki, A. Takeda, M. Miyamura, T. Ueno, T. Terai, K. Hanaoka, Y. Urano, T. Mineno, T. Nagano, *Chem. Commun.* **2011**, *47*, 10055–10057.
[28] a) Y. Gabe, Y. Urano, K. Kikuchi, H. Kojima, T. Nagano, *J. Am. Chem. Soc.* **2004**, *126*, 3357–3367; b) Y. Urano, D. Asanuma, Y. Hama, Y. Koyama, T. Barrett, M. Kamiya, T. Nagano, T. Watanabe, A. Hasegawa, P. L. Choyke, H. Kobayashi, *Nat. Med.* **2009**, *15*, 104–109.
[29] a) B. Roubinet, C. Massif, M. Moreau, F. Boschetti, G. Ulrich, R. Ziessel, P.-Y. Renard, A. Romieu, *Chem. Eur. J.* **2015**, *21*, 14589–14601; b) D. Hablot, A. Harriman, R. Ziessel, *Angew. Chem. Int. Ed.* **2011**, *50*, 7833–7836; *Angew. Chem.* **2011**, *123*, 7979–7982.
[30] a) G. Ulrich, R. Ziessel, A. Harriman, *Angew. Chem. Int. Ed.* **2008**, *47*, 1184–1201; *Angew. Chem.* **2008**, *120*, 1202–1219; b) R. Ziessel, G. Ulrich, A. Haefele, A. Harriman, *J. Am. Chem. Soc.* **2013**, *135*, 11330–11344.
[31] a) F. Zhong, A. Karatay, L. Zhao, J. Zhao, C. He, C. Zhang, H. G. Yaglioglu, A. Elmali, B. Küçüköz, M. Hayvali, *Inorg. Chem.* **2015**, *54*, 7803–7817; b) M. A. Miller, B. Askevold, K. S. Yang, R. H. Kohler, R. Weissleder, *ChemMedChem* **2014**, *9*, 1131–1135.
[32] a) F. Geist, A. Jackel, R. F. Winter, *Inorg. Chem.* **2015**, *54*, 10946–10957; b) T. Sun, X. Guan, M. Zheng, X. Jing, Z. Xie, *ACS Med. Chem. Lett.* **2015**, *6*, 430–433; c) B. Bertrand, P.-E. Doulain, C. Goze, E. Bodio, *Dalton Trans.* **2016**, DOI: 10.1039/c5dt04275e.
[33] a) G. Qing, C. Huabing, Z. Y. Lin, H. Hui, R. Jiaming (Suzhou University), CN105198934A, **2015**; b) P. Majumdar, X. Yuan, S. Li, B. L. Guennic, J. Ma, C. Zhang, D. Jacquemin, J. Zhao, *J. Mater. Chem. B* **2014**, *2*, 2838–2854.
[34] a) Q.-X. Zhou, W.-H. Lei, Y.-J. Hou, Y.-J. Chen, C. Li, B.-W. Zhang, X.-S. Wang, *Dalton Trans.* **2013**, *42*, 2786–2791; b) S. Tasan, O. Zava, B. Bertrand, C. Bernhard, C. Goze, M. Picquet, P. L. Gendre, P. Harvey, F. Denat, A. Casini, E. Bodio, *Dalton Trans.* **2013**, *42*, 6102–6109; c) P.-E. Doulain, R. Decréau, C. Racoeur, V. Gonclaves, L. Dubrez, A. Bettaieb, P. L. Gendre, F. Denat, C. Paul, C. Goze, E. Bodio, *Dalton Trans.* **2015**, *44*, 4874–4883.
[35] R. Lincoln, L. E. Greene, K. Krumova, Z. Ding, G. Cosa, *J. Phys. Chem. A* **2014**, *118*, 10622–10630.
[36] T. Lazarides, T. M. McCormick, K. C. Wilson, S. Lee, D. W. McCamant, R. Eisenberg, *J. Am. Chem. Soc.* **2011**, *133*, 350–364.
[37] U. Basu, I. Pant, I. Khan, A. Hussain, P. Kondaiah, A. R. Chakravarty, *Chem. Asian J.* **2014**, *9*, 2494–2504.
[38] B. Sarkar, R. Hübner, R. Pattacini, I. Hartenbach, *Dalton Trans.* **2009**, 4653–4655.
[39] W. Wu, J. Sun, X. Cui, J. Zhao, *J. Mater. Chem. C* **2013**, *1*, 4577–4589.
[40] C. Zhang, J. Zhao, S. Wu, Z. Wang, W. Wu, J. Ma, S. Guo, L. Hang, *J. Am. Chem. Soc.* **2013**, *135*, 10566–10578.
[41] H. Jia, B. Küçüköz, Y. Xing, P. Majumdar, C. Zhang, A. Karatay, G. Yaglioglu, A. Elmali, J. Zhao, M. Hayvali, *J. Mater. Chem. C* **2014**, *2*, 9720–9736.

[42] a) M. Fujii, M. Usui, S. Hayashi, E. Gross, D. Kovalev, N. Kunzner, J. Diener, V. Y. Timoshenko, *J. Appl. Phys.* **2004**, *95*, 3689 – 3693; b) S. Bystryak, I. Goldiner, A. Niv, A. M. Nasser, L. Goldstein, *Anal. Biochem.* **1995**, *225*, 127 – 134.
[43] Gaussian 09, Revision D.01, M. J. Frisch, et al., Gaussian, Inc., Wallingford, CT, **2009** (see the Supporting Information for full citation).
[44] A. D. Becke, *Phys. Rev. A* **1988**, *38*, 3098 – 3100.
[45] A. D. Becke, *J. Chem. Phys.* **1993**, *98*, 5648 – 5652.
[46] L. Yang, Y. Liu, W. Liu, C. Ma, C. Zhang, Y. Li, *Bioorg. Med. Chem. Lett.* **2015**, *25*, 5716 – 5719.
[47] N. M. Shavaleev, S. Davies, H. Adams, J. Best, J. A. Weinstein, *Inorg. Chem.* **2008**, *47*, 1532 – 1547.
[48] T. Mosmann, *J. Immunol. Methods* **1983**, *65*, 55 – 63.
[49] a) C. Frezza, S. Cipolat, L. Scoranno, *Nat. Protoc.* **2007**, *2*, 287 – 295; b) D. A. Clayton, G. S. Shadel, *Cold Spring Harb. Protoc.* **2014**, DOI: 10.1101/pdb.prot080002.
[50] M. Price, D. Kessel, *J. Biomed. Opt.* **2010**, *15*, 0516051.
[51] E. Gottlieb, S. M. Armour, M. H. Harris, C. B. Thompson, *Cell Death Differ.* **2003**, *10*, 709 – 717.
[52] L. B. Chen, *Annu. Rev. Cell Biol.* **1988**, *4*, 155 – 181.
[53] S. W. Perry, J. P. Norman, J. Barbieri, E. B. Brown, H. A. Gelbard, *BioTechniques* **2011**, *50*, 98 – 115.
[54] L. F. Marques-Santos, V. M. Coqueiro, V. M. Rumjanek, *Cell Biol. Int.* **2006**, *30*, 197 – 204.
[55] D. C. Joshi, J. C. Bakowska, *J. Vis. Exp.* **2011**, *51*, e2704.
[56] N. N. Danial, S. J. Korsmeyer, *Cell* **2004**, *116*, 205 – 219.
[57] I. Vermes, C. Haanen, H. Stefens-Nakken, C. Reutelingsperger, *J. Immunol. Methods* **1995**, *184*, 39 – 51.
[58] K. Million, E. Horvilleur, D. Goldschneider, M. Agina, G. Raguénez, F. Tournier, J. Bénard, S. Douc-Rasy, *Int. J. Oncol.* **2006**, *29*, 147 – 154.
[59] D. D. Perrin, W. L. F. Armarego, D. R. Perrin, *Purification of Laboratory Chemicals*, Pergamon Press, Oxford, **1980**.
[60] N. M. Shavaleev, Z. R. Bell, T. L. Easun, R. Rutkaite, L. Swanson, M. D. Ward, *Dalton Trans.* **2004**, 3678 – 3688.
[61] B. W. Michel, A. R. Lippert, C. J. Chang, *J. Am. Chem. Soc.* **2012**, *134*, 15668 – 15671.
[62] J. H. Price, A. N. Williamson, R. F. Schramm, B. B. Wayland, *Inorg. Chem.* **1972**, *11*, 1280 – 1284.
[63] J. Moussa, L.-M. Chamoreau, A. D. Esposti, M. P. Gullo, A. Barbieri, H. Amouri, *Inorg. Chem.* **2014**, *53*, 6624 – 6633.
[64] I. Carmichael, G. L. Hug, *J. Phys. Chem. Ref. Data* **1986**, *15*, 1.

Received: June 24, 2016
Published online on ■■ ■■, 0000

Light on target: Platinum(II) catecholates with 4,4-difluoro-4-bora-3a,4a-diaza-*s*-indacene (BODIPY)-appended pyridylbenzimidazole ligands specifically target mitochondria. The complexes exhibit remarkable photocytotoxicity in visible light in HaCaT cells by causing apoptotic cell death through singlet oxygen species, yet they are non-toxic in the dark. The emisssive BODIPY complex was used for cellular imaging, whereas the diiodo-BODIPY analogue showed remarkable photodynamic therapy effects.

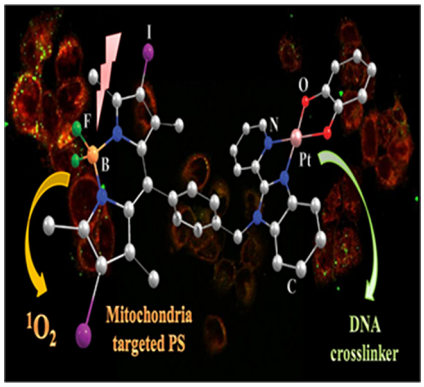

K. Mitra, S. Gautam, P. Kondaiah, A. R. Chakravarty**

■■ – ■■

BODIPY-Appended 2-(2-Pyridyl)benzimidazole Platinum(II) Catecholates for Mitochondria-Targeted Photocytotoxicity

These are not the final page numbers! ↗↗